Theoretical and Experimental Investigation of Indoor Flying Models*

MAX HACKLINGER

German Air and Space Research Establishment, Mechanics of Flight Institute

Summary:—*The development of a special model aeroplane technique is reviewed which renders possible easy and illustrative experimenting in the Reynolds number régime from 1 to 5000. The models are built in extremely light-weight construction; with wing span from 0·1 to 1 metre and all-up weights from 0·01 to 2 grammes, flight velocities between 0·1 and 1 m/sec are reached. The requirement of extremely low wing loading, together with the special air flow characteristics in this region, leads to rather unconventional construction principles with the materials balsa wood, nichrome wire and cellulose film. These principles are reviewed briefly. The problem of optimum propulsion for such model aeroplanes is treated analytically. Some results are given for flight performance optimisation. By combining theory and experiment there has been evolved, e.g. the Schwebeleistungs method (power required for horizontal flight) for optimising the duration of indoor model aeroplanes without exact knowledge of their aerodynamic characteristics. Flight characteristics with some elasticity of the structure present formidable problems and are reviewed in some examples. Finally, some problems of hangar meteorology are mentioned.*

1. INTRODUCTION

Aircraft of extremely low velocity have hitherto—apart from a few zoological studies of insect flight—remained largely ignored by aeronautical research. One of the reasons for this is that scarcely any essential technical application for this extreme region has been reported. Another is that experiments in this region necessitate unconventional techniques, which have already been developed in the small sphere of indoor flying model design but are unknown to aeronautical science.

On the other hand, this region is in many respects of interest to aeronautical science; the flow condition here lies in a region not well explained by published theories; here neither inertia nor viscosity may be neglected. Nothing is available here other than favourable experimental possibilities: flight testing becomes easier to perform, as mass and velocity decrease, and in many cases the difficult power measurement may be replaced by time and flight path measurements.

Table I gives a summary of the order of magnitude of indoor flying model characteristics in comparison with aircraft characteristics. The FAI established an indoor flying model class in about 1936 simply by restricting the wing span to 90 cm and recording the flight duration. Some of the following problems are defined by this particular requirement.

Notation

C_L lift coefficient
C_m pitching moment coefficient
C_D drag coefficient
C_{D_b} drag coefficient of bracing wire
C_{D_i} induced drag coefficient
C_{D_o} profile drag coefficient
E modulus of elasticity (in section 2 only)
E work (elsewhere)
S total lifting surface
S_b frontal area of bracing wires
W total flying weight
W_M weight of motor
h height
H ceiling
H_E energy height
K_1 constant in equation (9)

**Lecture given at the Annual WGL Meeting in Braunschweig, 9th-12th October 1962. Translated from the German by John B. Knight, B.Sc.(Eng.), Grad.R.Ae.S., British European Airways.*

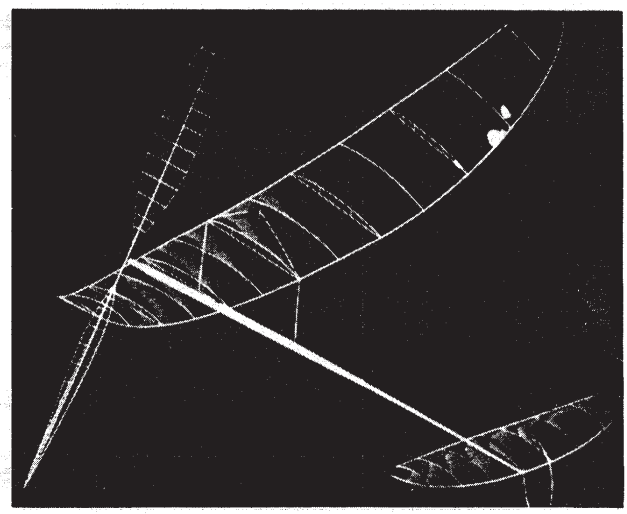

Photograph by Kaczmierczak

Figure 1. An FAI indoor model. Span 88 cm. Length 76 cm. Weights in grammes: fuselage 0·35, tail 0·07, wing 0·30, propeller 0·16, rubber 1·20.

K_3 constant in equation (27)
$\bar{c}$ mean wing chord
P power
Q propeller torque
n propeller speed
N number of turns used
l_T tailplane moment arm
R area ratio
R_e Reynolds number
$SM = -dC_m/dC_L$, "static margin"
t time
T duration
F fuel consumption per second
V flying speed
v_h horizontal speed
w rate of climb
w_s sinking speed
x distance between centre of gravity and neutral point in x-direction
z distance between centre of gravity and neutral point in y-direction

TABLE I

Summary of the Order of Magnitude of Indoor Flying Model Technology in Comparison with Other Aircraft

Quantity to be compared	*Dimension*	*Order of Magnitude*		
		Indoor model	*Sailplane*	*Obtainable at present time*
Flying speed	metres/sec	10^{-1} ... 1	10 .. 10^2	10^3
Flying weight	kilogram	10^{-4} ... 10^{-3}	10^2	10^5
Span	metres	10^{-1} ... 1	10	$5 \cdot 10^1$
Reynolds number	—	$5 \cdot 10^3$	$2 \cdot 10^6$	
Relative density	—	10^{-1}	4·10	10^8 10^2

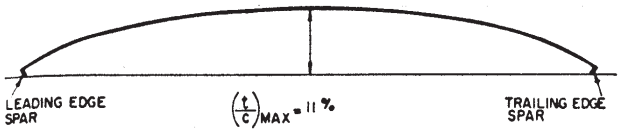

Figure 2. Actual indoor model aerofoil used for flow observation using smoke.

α angle of attack
γ specific weight
ε downwash angle
η propeller efficiency
$\mu = 2m/\rho S\bar{c}$, aircraft non-dimensional density ratio

Suffices

W wing
R rubber
T tailplane
O initial value or final value
H horizontal flight at $(C_L^3/C_D^2)_{max}$
A airframe

2. STRENGTH

The wing of the competition model demonstrated is of 90 cm span, weighs about 0·3 gr and has a proof load factor of about 3, for a flying weight of 2 gr. For such an extremely light component all known sheet wood and covering materials are too heavy. The construction must be divided into a primary and a supporting framework and a covering, which simply carries the aerodynamic loads. This covering consists of a cellulose film about 0·2μ thick, which is prepared by pouring onto a water surface.

The framework is so devised that nearly all parts are designed for buckling or wrinkling. The controlling parameter for this is E/γ^2 or E/γ^3. Table II shows the quantity E/γ^2 for several different materials. From this, balsa would undoubtedly be judged the most suitable material.

A completely opposite choice of material is necessary, however, for tension members. With the extremely lightweight construction developed in indoor flying model design, pure tension members only in the form of bracing are used. On account of the high drag coefficient $C_D = 10$ the optimum material is that with the highest tensile strength (chrome-nickel steel, Wolfram).

3. AERODYNAMICS

The air flow round a typical indoor flying model would be characterised by the following Reynolds numbers:—

Bracing	0·3 to 1·0
Spars and struts	100
Wing	5000

As an average of 0·7 revolutions per second, the airscrew lies in the Reynolds number region of the wing.

The particular characteristics of balsawood make possible a very simple and reliable method of measuring the drag coefficient of cylinders at low Reynolds numbers. From light indoor model balsawood, strips up to 0·2 mm thickness can be made. These descend in still air in a constant horizontal position, without deformation, and the condition is steady practically immediately. From the sinking speed and the weight of the strip one can obtain the drag coefficient up to about $R_e = 2$ free from wind tunnel turbulence and other constraints. For a homogeneous strip of diameter d that falls with constant speed V, one obtains, independently of the length of the strip

$$C_D = \gamma d\pi / 2\rho V^2 \quad . \quad . \quad . \quad . \quad (1)$$

without weighing.

From theoretical considerations and from several small investigations, it is known that the curved plate is preferable for all indoor model wing sections, and from measurements of glide performance (*see* section 5.2) it is known that a section symmetrical about the mid-chord with increasing camber towards the edges is better than a parabolic arc (*e.g.* Gö 417*a*). Unfortunately there is a total lack of accurate detail of optimum camber, etc. in this Reynolds number region.

From wind tunnel research on a model wing of aspect ratio 3·3, which was provided with spars on the under-surface, flow visualisation using smoke has shown the following unexpected phenomena: at an angle of incidence of 30° (measured from a thread) attached flow was observed on the upper surface up to about 85 per cent chord; on the lower surface the flow was, of course, attached up to the trailing edge. In general, these phenomena are supported qualitatively by flight observations of indoor flying models, by attaining similar high angles of incidence without stalling. The associated C_L is significantly smaller (about 1·0) than one would expect from theory.

Further, on the model wing centre line at $\alpha = 8°$ just behind the nose on the upper surface, a distinct lateral movement of the smoke was observed beneath the smoothly flowing mass of smoke, indicating a cross flow, which disappears with increasing angle of incidence.

To obtain the polars of an indoor flying model the gliding performance of an FAI indoor model must be measured. For this the propeller and rubber motor are replaced by trimming loads. By varying the trim, a C_L range of 0·15 to 0·97 can be measured in steady flight. Fig. 3 shows the velocity polar thus obtained, and Fig. 4 the lift-drag polar for the complete model calculated from this with the assumption $C_{LT} = 0·5$.

To detect the effect of Reynolds number, a model with a specially low wing chord was built and flight measurements made with weights on the centre of gravity in steps until loaded to the elastic limit. In this way a Reynolds number range of 3100 to 7300 was examined. Figs. 5 and 6 show that for the aerofoil used the Reynolds numbers in this region have considerable effect on the sinking speed parameter.

The propeller of the indoor flying model is—apart from the complicated matching of power and airframe—an aerodynamic-optimum problem which can be solved primarily with the help of a rotating arm and then by the practical horizontal-flight-power-measurement method (*see* section 5.2). Fig. 7 shows an indoor model propeller plan form designed by standard aircraft propeller potential theory.

Because the boundary layer is displaced by centrifugal force, the inner part of the blade can be more heavily loaded; this gives rise to a somewhat larger blade chord towards the tips and simultaneously a decreasing angle of incidence outwards, and therefore deviation from the geometric pitch. The propeller of the model shown has been developed in this way; for the horizontal flight power condition it has an efficiency of 0·77 (*see* section 5.2).

TABLE II
E/γ^2 for Several Different Materials

Steel	$0·34 \times 10^8$ cm^4/gr
Fibreglass	$0·95 \times 10^8$ cm^4/gr
Dural	1×10^8 cm^4/gr
Pine	5×10^8 cm^4/gr
Medium balsa	19×10^8 cm^4/gr

4. DRIVE

From a comparison of different drives, Fig. 8 shows the characteristic power curve for a typical indoor flying model rubber motor. The effective work from rubber is

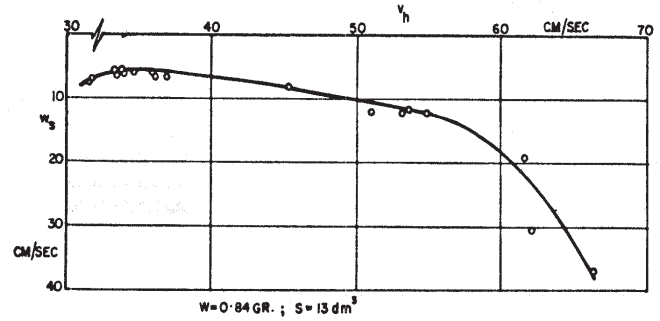

Figure 3. Velocity polar of an indoor model from glide measurements.

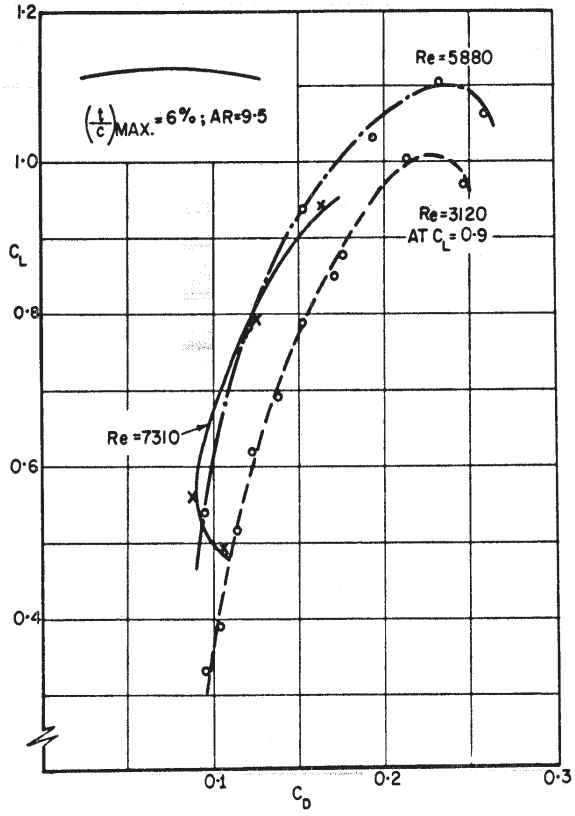

Figure 5. Effect of Reynolds Number on the complete model polars from glide measurements.

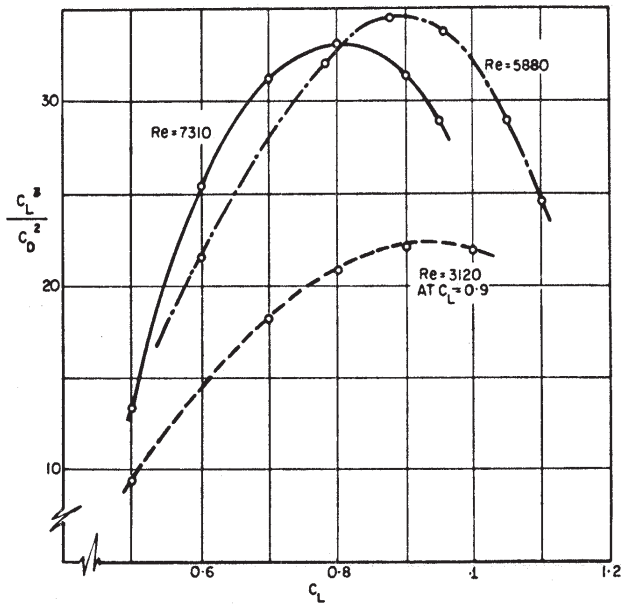

Figure 6. Effect of Reynolds Number on the climb parameter (from Fig. 5).

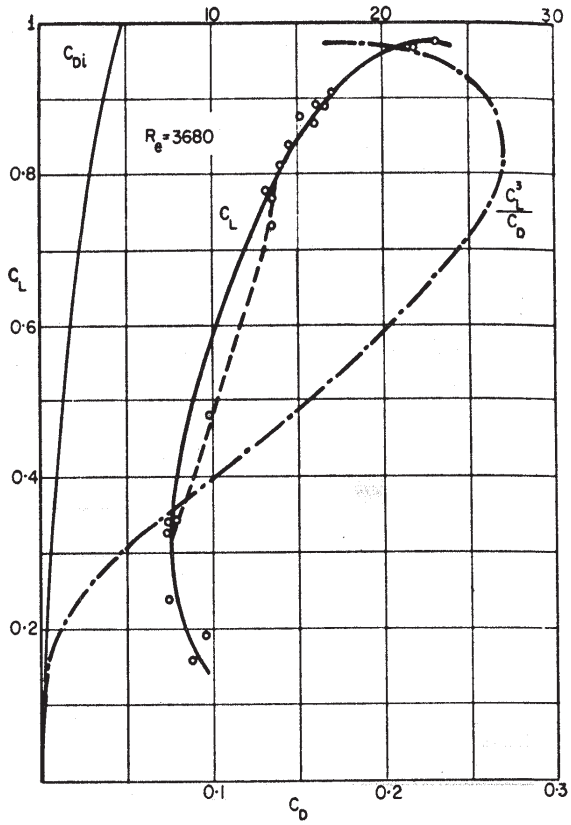

Figure 4. Complete model polars of an indoor model from glide measurements (from Fig. 3).

$$E=\int Q\omega dt=\int Q\,.\,2\pi\,.\,n\,.\,dt \quad . \quad . \quad (2)$$

The relation between propeller speed n and the number of revolutions N used is

$$n=dN/dt. \quad . \quad . \quad . \quad . \quad (3)$$

Hence

$$E=2\pi\int QdN. \quad . \quad . \quad . \quad . \quad (4)$$

In relation to the flight duration, the power is optimum when the energy height

$$H_E=\frac{\text{work}}{\text{weight of the motor}} \text{ is maximum.}$$

From several measurements it is shown that H_E for indoor flying model rubber motors is approximately constant with

$$H_E=900\ m. \quad . \quad . \quad . \quad . \quad (5)$$

With the use of rubber motors, the flying weight remains constant but the torque varies greatly, while for the internal combustion motor Q=constant, $W \neq$ constant. We define the energy height of internal combustion motors as

$$H_E=\int\frac{Pdt}{W(t)}=P\int\frac{dt}{W(t)} \quad . \quad . \quad (6)$$

$$W(t)=\underset{\text{motor weight}}{W_M}+\underset{\text{fuel weight}}{W_F}+\underset{\text{fuel consumption}}{Ft}. \quad . \quad . \quad (7)$$

Integration between $t=0$ and $t=T$, where $FT=W_F$ gives

$$H_E=\frac{P}{F}\log_e\left(1+\frac{FT}{W_M}\right)$$

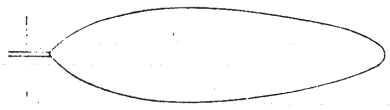

Figure 7. Propeller blade shape for indoor models from potential flow theory (Theodorsen).

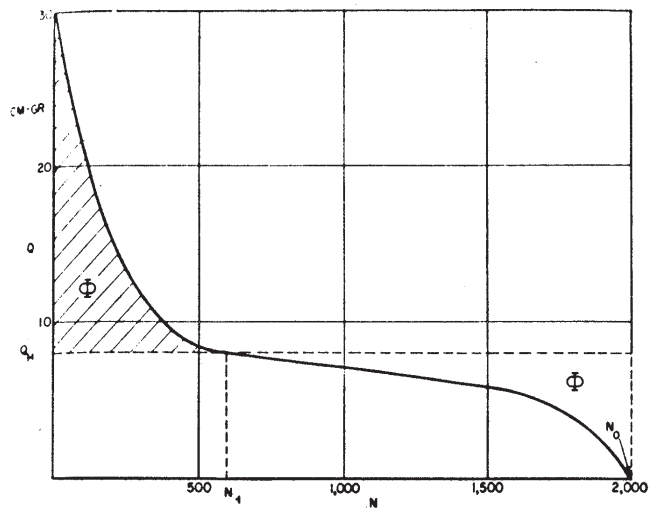

Figure 8. Work curve of a rubber motor (twisted strands of rubber).

or with specific consumption

$$H_E = \frac{1}{F_{sp.}} \log_e \left(1 + \frac{F_{sp.}}{W_M/P} \cdot T\right). \quad . \quad . \quad (8)$$

Putting the usual values for $F_{sp.}$ and W_M/P for internal combustion motors, and comparing the energy heights from (5) and (8), shows that flying time for which the internal combustion engine and the rubber motor are equally good, namely $T=6{\cdot}3$ sec.

For longer flights the internal combustion motor—for shorter flights the rubber motor—is preferable. The reason that one can nevertheless achieve high durations of about 45 min with indoor flying models, where no internal combustion engines are used, is found in the dead weight of the motor which with a reasonable model size need only amount to a few grammes. Similarly, for the electric motor. Recently suitable sources of power became available, but for indoor flying models the motor weight is still too high. Rocket power has a very low dead weight, but it has been eliminated because hitherto it has not been able to achieve constant rate of combustion over the long flight durations.

In addition, the all-wing flying model demonstrated* of 25 cm wing span has a horizontal flight power requirement of $4{\cdot}10^{-8}$ h.p.

5. FLIGHT PERFORMANCE

5.1. Combination of Power and Airframe

The flight of an FAI indoor flying model, when analysed using the power characteristic of Fig. 8, has the path shown in Fig. 9. With a fixed pitch propeller the energy utilisation is optimum when the motor is just run down at landing (run down condition).

The first part of the problem is the amount of power. By applying a choice of propellers, the just-run-down stipulation can be met with different rubber motors. We state first that the model flies at its optimum sinking speed parameter for all values of torque. In practice this is achieved by varying the choice of pylon height, spiral stability, direction of propeller thrust, and so on. Then, at the climbing speed:

$$w = \frac{P\eta}{W} - \sqrt{\left(\frac{2WC_D^2}{\rho S C_L^3}\right)} = \frac{P\eta}{W} - K_1\sqrt{W} \quad . \quad (9)$$

With $P=dE/dt$ the equation of the flight path follows therefrom:

*This model was shown at Braunschweig and is mentioned here because of its exceptionally low power requirement.

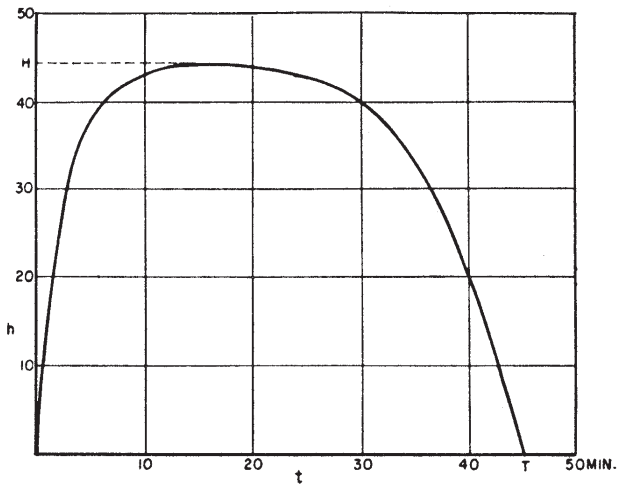

Figure 9. Typical flight pattern of an FAI indoor model.

$$\frac{dh}{dt} = \frac{\eta}{W} \cdot \frac{dE}{dt} - K_1\sqrt{W} \quad . \quad . \quad . \quad (10)$$

Hence

$$t = \frac{E\eta/W - h + K_2}{K_1\sqrt{W}} \quad . \quad . \quad . \quad . \quad (11)$$

We have the limiting conditions

for $t=0$ $E=0$.

$h=0$ $K_2=0$

for $t=T$ $h=0$

$E=H_E W_R = H_E(W-W_A)$.

From this equation (11) becomes

$$T = \frac{H_E \cdot W_R \cdot \eta}{K_1 W^{1.5}} \quad . \quad . \quad . \quad . \quad . \quad (12)$$

Since $dT/dW=0$, $W_R/W_A=2$. . . . . (13)

Figure 10 shows that this maximum has a very flat shape and it is clear, therefore, that even very small side-effects, such as the increase in fuselage weight with a stronger motor, causes a significant shift to a smaller propulsion component.

The flight ceiling found from optimum propulsion con-

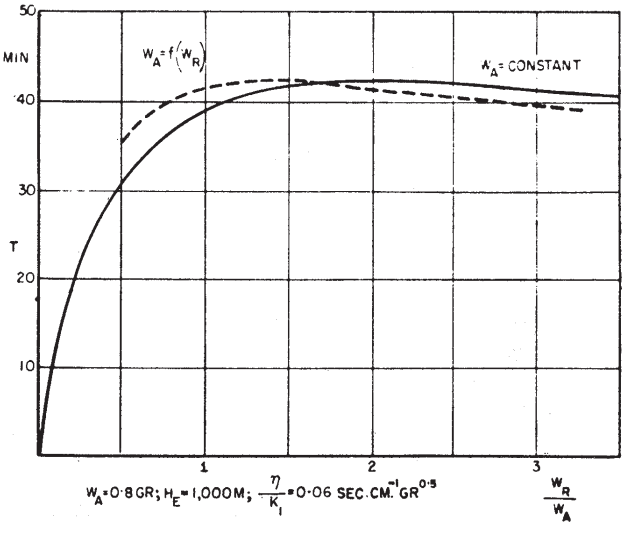

Figure 10. Effect of motor weight on flight duration.

siderations normally exceeds the vertical height of the available halls; therefore the consideration of the altitude is a further important part of the problem. From equation (11)

$$h=(\eta E/W)-w_s t \quad . \quad . \quad . \quad (14)$$

or for the maximum height

$$H=(\eta E_H/W)-w_s T_H. \quad . \quad . \quad . \quad (15)$$

$E=2\pi\int_0^{N_H} QdN$—work up to maximum height

T_H—elapsed time up to maximum height.

For horizontal flight (at $(C_L^3/C_D^2)_{max.}$)

$$Ww_s=\eta \,.\, 2\pi \,.\, Q_H \,.\, n_H \quad . \quad . \quad . \quad (16)$$

therefore

$$w_s \,.\, T_H=\frac{2\pi\eta}{W} \,.\, Q_H \,.\, n_H \,.\, T_H. \quad . \quad . \quad (17)$$

With $n_H \,.\, T_H=N_H$ it follows from equations (15) and (17)

$$H=\frac{2\pi\eta}{W}\int_0^{N_H}(QdN-Q_H \,.\, N_H)=\frac{2\pi\eta}{W} \,.\, \varphi. \quad . \quad (18)$$

Further, we obtain the average torque

$$\hat{Q}=\frac{1}{N_0}\int_0^{N_0} QdN. \quad . \quad . \quad . \quad (19)$$

Then, since the work $2\pi\phi$ available for the climb according to the run-down condition will be exactly recovered in the subsequent descent, the average torque $\hat{Q}$ will be equal to the torque in horizontal flight Q_H.

One can therefore—assuming a rigid model with constant efficiency and flying weight—obtain the ceiling for each rubber motor.

If R is the ratio of the area ϕ to the total area under the torque curve from Fig. 8, the height is:

$$H=\eta \,.\, \frac{W_R}{W} \,.\, H_E \,.\, R. \quad . \quad . \quad . \quad (20)$$

The usual range of R is about 0·15 to 0·28. When the model and propeller are considered together and it is required to find the rubber which will satisfy the run-down condition—without theory, a most tedious process—one must measure the horizontal flight torque with any rubber of known weight, and select from the statically measured torque curves that one which possesses the suitable $\hat{Q}$.

5.2. Total Flying Time Estimation

Since only small halls are available for most test flying, and the flights are of very long duration, the main problem is the estimation of the possible unlimited duration of an indoor flying model, without it flying to maximum ability. The calculation of this time is not possible with reasonable accuracy because of the uncertainty of the basic aerodynamic data. The following method has been found as a solution.

From equation (10) it follows for horizontal flight

$$\frac{dh}{dt}=0=\frac{\eta}{W} \,.\, P_H-K_1\sqrt{W}. \quad . \quad . \quad (21)$$

For the power P_H for horizontal flight substituting $2\pi Q_H \,.\, n_H$

$$\text{gives} \quad \frac{K_1}{\eta}=\frac{2\pi Q_H \,.\, n_H}{W^{1.5}}. \quad . \quad . \quad . \quad (22)$$

Substituting equation (22) in (12)

$$T=\frac{H_E W_R}{2\pi Q_H \,.\, n_H}. \quad . \quad . \quad . \quad . \quad (23)$$

The energy height of rubber is approximately constant and can be found from integration of the rubber power curve.

The horizontal power method is composed, therefore, of the following: to analyse an indoor flying model with an arbitrary rubber motor of weight W_R whose torque characteristic is unimportant, sufficient turns are given so that it just maintains horizontal flight. In this condition, by counting and using a stopwatch, the propeller speed n_H (about 0·7 rev per second) is determined, and subsequently Q_H is determined by a small torque-measuring device attached to the propeller shaft. With these data available one obtains possible total flying time from equation (23). With this procedure the difficult measurement of aerodynamic quantities is avoided and reduced to a simple observation (horizontal flight) and a time—and static torque measurement.

This method renders possible a range of study only possible hitherto with a great amount of research. Thus one can follow the results from changes in components; one could try propellers of different diameters or different pitches with the same rubber in the same model. One would then obtain widely differing particular values of Q_H and n_H, but

$$\Delta=\frac{(Q_H \,.\, n_H)_2-(Q_H \,.\, n_H)_1}{(Q_H \,.\, n_H)_1} \,.\, 100 \text{ per cent} \quad . \quad (24)$$

immediately gives by how much combination 2 is better than combination 1. In exactly the same way new wing sections, bracing, and so on, can be examined.

This method has also been used for the study of propeller efficiency, when combined with measurements in horizontal flight. From glide measurements without the propeller one gets K_1, from the horizontal flight power measurement $Q_H \,.\, n_H$ and from (22) we get η.

Equation (23) applies with the stipulation K_1=const. Accordingly the closest agreement between the results of the horizontal power measurement method and the actual flight duration would be expected when the model is bestowed with such characteristics that it maintains the required high angle of incidence throughout the whole flight.

5.3. Optimum Bracing

To optimise the duration of the flight the problem of bracing must also be considered. For aircraft or model aircraft which must be able to achieve long flights for a given amount of energy (by air currents or motors) the sinking speed must be correspondingly low. Therefore, is the cantilever or the braced structure more favourable?

From the study and comparison of many leading FAI-class indoor models, it has been determined how much wing weight can be saved through use of a certain amount of constant diameter bracing wire arranged in an optimum configuration. This is shown in Fig. 11, which agrees closely with

$$W=\frac{a_1}{(S_b+a_2)^\nu}+a_3 \quad [\text{gr}] \quad . \quad . \quad . \quad (25)$$

The coefficients have the values a_1=0·1032, a_2=0·176, ν=1·48, a_3=1·85.

The sinking speed is

$$w_s=\sqrt{\left(\frac{2WC_D^2}{\rho S C_L^3}\right)}=\sqrt{\left(\frac{2W}{\rho S C_L^3}\right)}\left(C_{D_0}+C_{D_i}+C_{D_b} \,.\, \frac{S_b}{S}\right). \quad (26)$$

Substituting equation (25) in (26) gives

$$w_s=K_3\left(\frac{a_1}{(S_b+a_2)^\nu}+a_3\right)^{0.5}\left(C_{D_0}+C_{D_i}+C_{D_b} \,.\, \frac{S_b}{S}\right). \quad (27)$$

With $C_{D_0}+C_{D_i}$=0·14; C_{D_b}=10; S=13 dm^2, from Fig. 12 the optimum amount of bracing is 0·6 cm²; this is 6 metres of

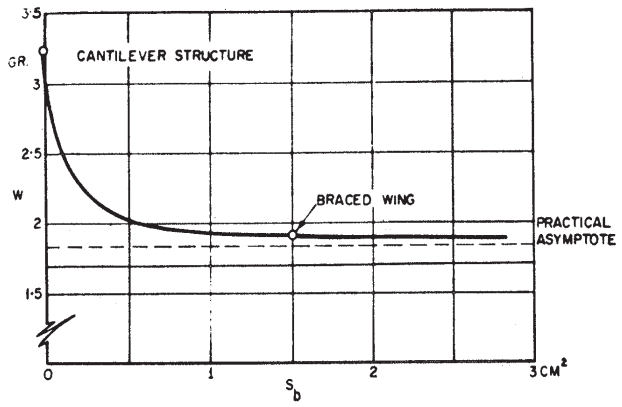

Figure 11. Weight saving due to bracing on FAI indoor models.

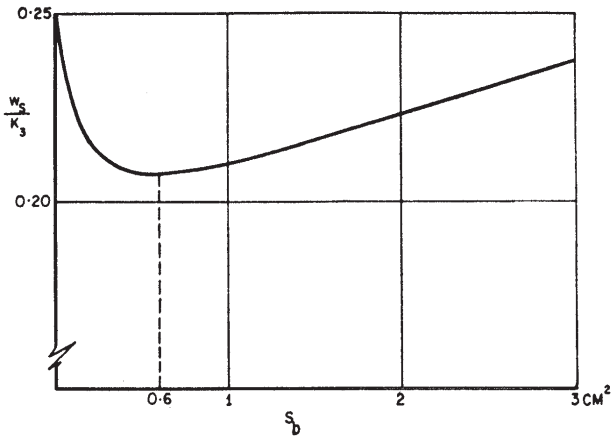

Figure 12. Effect of bracing on the sinking speed from (27).

0 012 mm diameter chrome-nickel wire. The limiting value for $dw_s/dS_b=0$ can be directly calculated from equation (27), but this gives a very unwieldy expression.

The relation between W and S_b for aircraft is similar to that shown in Fig. 11 and as the wire drag coefficient there is much more favourable, a positive optimum value of S_b is also obtained for light aircraft. This applies particularly to man powered aircraft.

5.4. Tailplane Discussion

A further part of the problem of flight efficiency and flight characteristics is the configuration of the tailplane. We can write for the sinking speed

$$w_s=\sqrt{\left(\frac{2W}{\rho}\frac{(C_{D_W}\,.\,S_W+C_{D_T}\,.\,S_T)^2}{(C_{L_W}\,.\,S_W+C_{L_T}\,.\,S_T)^3}\right)}\quad .\quad . \qquad (28)$$

with $\quad C_{D_W}=C_{D_{oW}}+\frac{C_{L_W}^2}{\pi A_W};\quad C_{D_T}=C_{D_{oT}}+\frac{C_{L_T}^2}{\pi A_T}.$

This function is to be a minimum with the secondary condition of adequate stability. For static stability

$$dC_m/dC_L=-(\text{static margin})$$

$$=\frac{(h-h_N)}{\bar{c}}+\frac{z}{\bar{c}}\cdot\frac{dC_D}{dC_L}\,.-\left(\frac{d\alpha}{dC_L}-\frac{d\varepsilon}{dC_L}\right)\left(\frac{dC_L}{d\alpha}\right)_T\frac{S_T\,.\,l_T}{S_W\,.\,\bar{c}} \qquad (29)$$

with $$\frac{dC_L}{d\alpha}=\frac{6A}{A+2};\quad \frac{d\varepsilon}{dC_L}=\frac{2}{A_W\,.\,\pi}\quad .\quad . \qquad (30)$$

and making the usual simplification that $SM \ll l_T$,

$$\frac{S_T}{S_W}=\frac{SM}{\frac{l_T}{\bar{c}}\left(\frac{A_W-1{\cdot}82}{A_W}\cdot\frac{A_T}{A_T+2}-\frac{C_{L_T}}{C_{L_W}}\right)}\quad .\quad . \qquad (31)$$

Figure 13 shows the relation between C_{L_T} and SM from equation (31) and the relation between sinking speed and tailplane size for two typical indoor models. Because of shortage of time, the complete effect can still not be determined from equations (28) and (31) because the precise effect of tailplane weight is missing. One can, however, say that relatively large tailpanes, which fly at $C_{L_T}=0{\cdot}6\ C_{L_W}$, are preferable to symmetrical ones.

6. FLIGHT CHARACTERISTICS

The basic flight characteristics of indoor flying models differ from those of free flight models and aircraft. The essential difference is the low aircraft relative density $\mu=2m/\rho S\bar{c}$. For comparison:

For a transport aircraft	$\mu=100$
For a sailplane	$\mu=40$
For an indoor model	$\mu=0{\cdot}1$ to $0{\cdot}2$.

Relative to the aircraft mass the indoor model affects a large mass of air, so that even after strong disturbances a steady condition is quickly established. On the other hand, the motion of the aircraft is more strongly affected by the motion of the surrounding mass of air. In aircraft gust calculations the effect of the accelerated air mass, which is accounted for by taking an air cylinder of span times chord, usually is one order of magnitude smaller than the other two parts of the gust-air load. While for sailplanes this only amounts to about 1/30 of the flying weight, for light indoor models it is ten times the weight of the whole model.

This could be the reason for the peculiar stalling behaviour of indoor models; after the maximum lift has been attained in steady flight, the model has two possibilities at the highest point of the flight path: downwards acceleration of the air mass influenced by the wing (as occurs with a stalled aircraft) or reversal of the circulation and backward flight. The second process needs less energy and is therefore chosen for the indoor flying model. Through variations of static stability it is possible to achieve this characteristic stalling behaviour in completely different forms. The fact that air damping is very high in relation to mass forces also explains the fact that indoor flying models cannot be made to spin, although the normal simplified flight-mechanical relations give stable autorotational conditions at very small values of μ. The precise solution of the unsteady aerodynamics involves difficult calculations and at present there is no complete solution.

The relatively small inertia forces resulting from the structure weight means, among other things, that loads arising from contact of models with solid objects do not result in loadings worth mentioning, aerodynamic forces alone being the decisive ones.

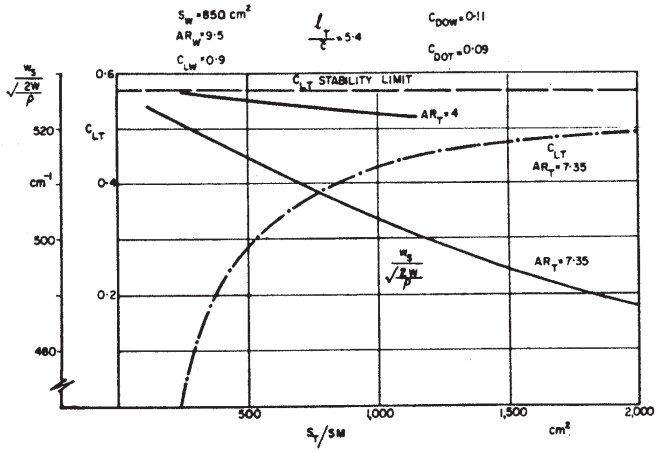

Figure 13. Effect of the tailplane on the sinking speed at a given degree of stability —C_{LT} as a function of S_T/SM at constant C_{LW}.

The large and widely varying thrust moment with indoor models causes the main problem of the asymmetric flight characteristics. For comparison with aircraft, we form the parameter Q/Wb (torque coefficient), where Q is the propeller torque at take-off power, W the flying weight, and b the semi-span. For a typical light aircraft the characteristic value is 0·009 compared with 0·37 for an FAI indoor flying model, that is, about a forty-fold increase.

To keep the loss due to side-slipping in steady turning flight small, several methods are available: enlargement of the vertical tail surface, offsetting the propeller thrust line, different aerofoil sections in each wing half, V-dihedral wing, asymmetrical wing plan form, wing twist, and so on.

The use of propeller side thrust scarcely affects the power, but when it is used solely to balance torque the lateral fuselage bending moment becomes unacceptably great.

Highly cambered aerofoils seem almost ideal for the wing on the inside of the turn, were it not for the unfavourable characteristic that the model stalls out of the turn.

The V-dihedral wing together with pylon-mounted wing is already adopted to achieve constant climb parameter during the whole flight. Otherwise the V-wing would be used as little as possible from performance considerations.

Asymmetrical wings and twist have different effects insofar as twist increases the induced drag because of the irregular shape of the lift distribution. Moreover, the balancing moment due to twist is dependent on the dynamic head, which with asymmetry, on the other hand, it is not (because in steady flight $L=W=$constant).

For the practical purpose we shall proceed as follows: for the radius of turn adopted for the model the variation of speed across the span is determined and the wing is twisted so that elliptic loading is re-established. This twisted wing will then be offset from the fuselage axis by an amount $e=Q_H/W$ so that the rolling moment in horizontal flight is just cancelled. Thus for the greater part of the flight, sideslipping, which the propeller would otherwise cause, will be prevented without an increase of drag.

Oddly enough, the determination of the propeller diameter comes under the heading of flight characteristics. This is not limited on structural grounds, and from efficiency considerations it would need to be made as large as possible. It appears, however, that above a certain propeller diameter, because of the asymmetric periodic influence of the wing flow by the propeller wake, nutational oscillations arise, which impair the performance. From practical experience the limiting values are about $d=0{\cdot}53-0{\cdot}58\ b$ (d=diameter, b=wing span); it depends to some extent on the pitch and with increasing pitch the value becomes smaller. Because of the small mass (weight of a propeller of diameter 50 cm: 0·15 gr) the effect of the gyroscopic force on the flight characteristics is negligible. On the other hand, the "propeller fin effect" is important. The advance ratio, load factor, diameter and blade width are required to determine this theoretically. For an FAI indoor model this calculation for the horizontal flight performance (at $(C_L^3/C_D^2)_{max}$), and consequently for the longest part of the flight, shows that the effect of the propeller on stability is as though a surface of the same span and half the chord of the tailplane is placed at the position of the propeller. The setting of this destabilising surface corresponds to the direction of the propeller thrust axis.

7. INFLUENCE OF ELASTICITY

With such an extremely light structure as an indoor flying model it is to be expected that the critical stresses would arise from the influence of elasticity. Flutter with indoor models—because of the small inertia forces and large damping—is never observed. On the other hand divergence often occurs. This is the decisive wing-stressing case. Since the flight characteristics of indoor flying models can be accurately observed and often measured as well with little expenditure of time and labour, experiment leads to the optimum dimensions more quickly than calculation. The tailplane boom will also be determined by divergence; if the model flies backwards for a short time after stalling, the tailplane and tail-boom represent an intensely unstable configuration from the aeroelastic standpoint. On the other hand, aeroelastic effects can often be used with advantage to achieve favourable flight characteristics which cannot be obtained with the design parameters of rigid models. One example is the variable pitch propeller: for better utilisation of the high initial torque, indoor flying model propellers are often constructed with the flexural axis situated behind the centre of pressure, causing an increase of pitch. Another is the use of the torque dependent fuselage deflection for stabilisation of the initial climb or for altitude restriction.

The influence of an elastic tail boom on the longitudinal stability of indoor flying models is determined by calculation. In contrast to known aircraft investigations, the contribution of the tailplane load to the total load system cannot be neglected here, moreover, because of the low inertia of indoor flying models during a disturbance, the horizontal velocity changes so much that one dare no longer neglect these changes. The calculation, details of which cannot be given here, leads, among other things, to the result that an improvement of the longitudinal stability occurs with a known elasticity of the rear fuselage, when the condition

$$D\frac{C_{L_T}'}{C_{L_W}'}<\frac{C_{L_T}}{C_{L_W}} \qquad . \quad . \quad . \quad (32)$$

(where D=downwash factor)

is satisfied. For many indoor flying models the parameter from equation (32) is such that the elasticity of the fuselage is favourable. In these cases the dimensioning of the tail boom is in practice determined by the divergence case with reverse flow.

8. HALL METEOROLOGY

Unrestricted indoor free-flight performance of three quarters of an hour duration presupposes a very calm hall atmosphere, which may contain small scale turbulence, but no slow exchanges of air over a wide area. Apart from pressure differences due to stray currents, convective phenomena are chiefly responsible for this movement. Initially halls with double walls, like the Dortmund Westfalenhall, proved to be best, but from experience we found that simple corrugated iron airship hangars are more favourable. Probably the reason for this is the significantly greater temperature gradient in the vertical plane. The stabilisation of the air layers caused by this means is so strongly manifest that it overcomes the pressure differences due to artificial disturbances (leakage), which can be considerable with a simple hall. During their slow, steady circling flight indoor flying models are an excellent means of observing small currents in large rooms. In the Cardington (England) airship hangar in which the 1961 World Championships were conducted, for example, a certain horizontal oscillation of the air existing under the narrow warm ceiling (temperature 5°C higher than on the floor) could be observed. This occurred due to heating on one side and disturbances caused by the wind, not strong enough to cause the complete breaking up of air layers of the hall atmosphere (as occurred during a thunderstorm). The purely analytical treatment of such problems is extremely difficult because of the complexity of the associated convection currents. Together with suitably set-up flight investigations, it should, however, succeed in throwing some light on this most obscure part of the whole matter treated here.